1981

CONCRETE SCIENCE

Treatise on Current Research

V.S. RAMACHANDRAN
R.F. FELDMAN
J.J. BEAUDOIN

Division of Building Research
National Research Council
Canada

HEYDEN
LONDON : PHILADELPHIA : RHEINE

1 Microstructural aspects of cement paste

The structure of a porous body, constituting porosity, pore size distribution and size and shape of the solid material, largely determines the mechanical properties of that body. A consistent relationship between porosity and mechanical properties of hydrated Portland cement paste is normally observed, except at low porosities. If the mechanical properties are considered in terms of chemical forces between particles, the strength of the paste would then be related to the number of chemical bonds per unit volume, the bond strength and the strength of the particles themselves. The number of bonds should depend on the concentration, size and shape of the hydrated cement particles and these, in turn, are related to the absolute density and porosity of the paste. Attempts have also been made to study the solid phase of cement paste in terms of the morphology of the hydrated particles. In this chapter the primary factors related to the structure (viz. microstructural features as revealed by electron microscopy, bonding of the solid phase, porosity, pore shape, surface area and density) that are important to an understanding of the mechanical properties are emphasized.

1.1. SOLID PHASE

1.1.1. Microstructure from microscopic techniques

Microstructural studies of cement paste may be on several levels. Scanning electron microscopes are used to study the microstructure of cement paste at the individual particle level, since microunits formed in the cement paste are too small to be amenable to investigation by optical microscopes.

Radczewski *et al.*[1] were probably the first to apply the microscopic technique for investigating cementitious systems and since then several refinements to the technique have been made, resulting in the publication of innumerable micrographs which are contradictory and confusing.

It has been reported that, in paste products, (a) well-crystallized tobermorite plates are responsible for strength and the fibres and foils are poorly integrated; (b) the strength is a consequence of the highly colloidal structure of the product; or (c) the fibrous morphology is associated with strength. It is not easy to state whether a particular morphology is conducive to strength. Soon after mixing, ettringite crystals in supersulphated cement seem to contribute to strength whereas at later stages C-S-H gel contributes to strength. Gypsum, ettringite and magnesium oxychloride are acicular and the C-S-H gel is known to consist of fibrous particles and irregular plates. All yield good strengths. Morphologically, it is assumed that cubic C_3AH_6 with a low surface area gives poor strength but, under certain conditions of low water/solid ratio and higher temperatures, it produces a very strong product.[2] In autoclaved Portland cement–silica products, platy 11 Å tobermorite has been reported to contribute to strength, whereas the other product, αC_2S hydrate, also of platy morphology, is generally detrimental to strength development. These facts suggest that morphological features alone may not determine strength.

It is beginning to be recognized that comparison of micromorphological results by different workers has an inherent limitation because of the small number of micrographs usually published and the correspondingly small area represented by these micrographs, which might not be representative of the structure. What may be selected by one researcher as the representative structure may differ from that selected by another. Even the description of the apparently similar features becomes subjective.[3] Consequently, speculations on the origin of strength and other properties, when based on these observations, have limited validity, especially since many properties of cement paste are influenced at a much lower microlevel than can be observed by the electron microscope.

The microstructural features of a hydrating cement can be pictured as follows. In the early stages the micromorphology consists of an assemblage of hydrating cement grains separated by considerable space. As hydration progresses, it becomes difficult to distinguish individual units. Some areas containing plates of CH can be delineated but at maturity they become less distinct and the whole structure has a uniform appearance.

In spite of human and instrument limitations, electron microscopic techniques have provided useful information on morphological features and an estimate of the elements contained in the microunits of various products, especially for cements made at higher water/cement (w/c) ratios. In Fig. 1.1, the effect of $CaCl_2$ on the microstructural features of cement, C_3S and $C_3A + CaSO_4.2H_2O$ is shown. Addition of 2% $CaCl_2$ to cement results in a 50%

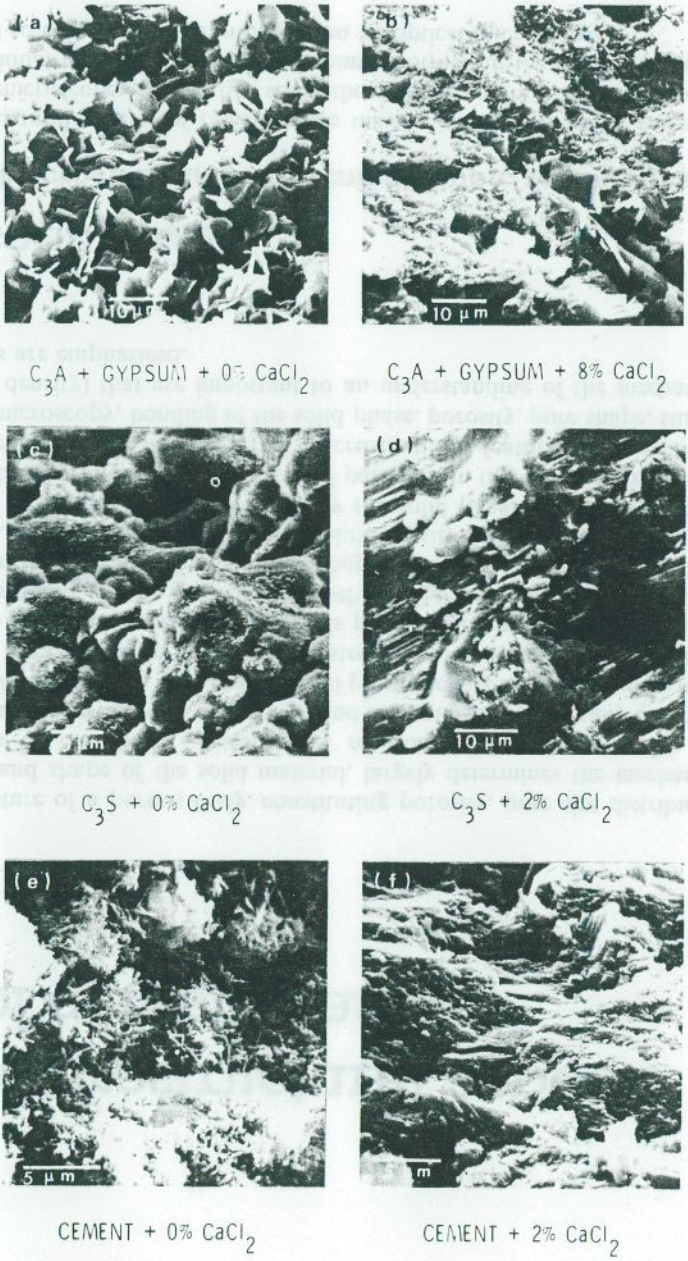

Figure 1.1. Microstructural development in cement containing calcium chloride.

increase in strength and is attended by a highly consolidated microstructure. A similar structure develops in $C_3S + CaCl_2$ pastes but with a 70% increase in strength. In the C_3A + gypsum system, treated with 8% $CaCl_2$, the strength increases by 100% and small needles and plates develop in place of platy structure.

1.1.2. Bond formation

The kinds of bonds existing in cement paste are not easy to resolve because bond strength is very difficult to measure. According to Rehbinder *et al.*,[4] in binders, crystallization contacts associated with the process of crystal coalescence are controlled by a given level of supersaturation. They also suggested that there is a balance between the supersaturation level in the surrounding medium and the mechanical effort necessary to maintain the crystals in a certain fixed position relative to each other. Thus, internal strain is related to the pressure associated with the constrained crystal growth. Under conditions conducive to reducing internal strain, strength would increase.

Sychev[5] considered structure formation as the synthesis of a solid body by condensation of a disperse system. He attempted to link the binding property of the hydrating system with products having polar groups. In this theory, the first step of hardening is supposed to be associated with the 'constrained state' when particles are brought together so close that long-range forces begin to act and the polar groups in the surfaces serve as a crystallization contact of valency type. This hypothesis suggests that bonds are based on the chemical attachment of water molecules and saturation of the ionic fields on the surfaces. According to Sychev, this bond can be strong only when most of the free water has been removed, resulting in a low concentration of water at the contact faces. This is possible during the accelerated stage of hydration.

Ubelhack and Wittman[6] proposed that a few molecular layers of water separate surfaces of most of the interparticle bond area. These water films, exhibiting a high degree of ordering due to surface interaction, cause a disjoining pressure. Wittman *et al.*[7] used Mossbauer spectra to obtain values of the coupling constant for hydrated cement paste. These values were found to decrease from 2×10^5 dyn/cm at 0% r.h. to 1.4×10^5 dyn/cm at 55% r.h. and to 0.8×10^5 dyn/cm at 100% r.h. These values are consistent with the concept that water enters the layered system as humidity is increased. The maximum value of the modulus of elasticity at 100% r.h. is due to water entering the interlayer positions and reinforcing the system by interaction with the two layers. Setzer and Wittman[8] consider that the strength of the hydrated paste originates partly from chemical bonding with no influence from water vapour, and partly from physical forces, constituting about 50% of the total bond strength. This estimate was based on calculations of the free energy change during water adsorption and the length change isotherm. These

procedures are not valid because they do not consider the sorption isotherm as the result of several phenomena including interlayer penetration and ageing.

None of these hypotheses seems to have considered the polymerization of SiOH groups as a process forming solid-to-solid contacts. Collepardi[9] proposed the formation of these groups from a study of changes in pore size and surface area. However, in other investigations it would be difficult to ascertain whether these result in intraparticle or interparticle bonds.

The role of sorbed water on bonding is discussed in Chapter 3 in terms of Young's modulus. It is shown that water sorbed in cement paste does not behave simply as adsorbed water but enters the bond area to reinforce it.

The exact structure of C-S-H is not easily found. Considering the several possibilities by which the atoms and ions are bonded to each other, a model may be constructed. Figure 1.2 shows a number of possible ways in which siloxane groups, water molecules and calcium ions may contribute to bonds across surfaces or in the interlayer position of poorly crystallized, malformed tobermorite-like material. In this figure vacant corners of the silica tetrahedra will be associated with cations.

By the technique of cold compaction and recompaction of hydrated cement, it has been shown that bodies can be fabricated which are similar in structure and mechanical properties to bodies formed in normal hydration.[10] The compaction process seems to produce interparticle bonds similar in nature to those produced by the hydration process. It is possible that microunits or

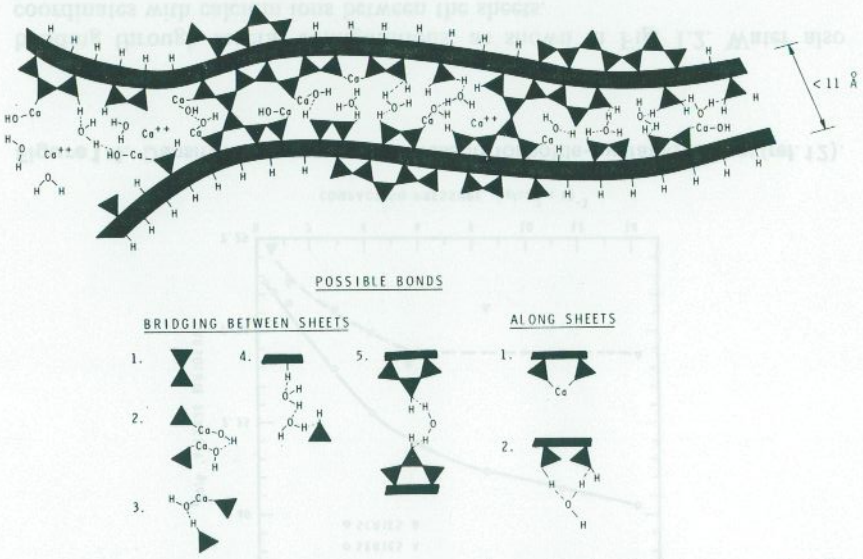

Figure 1.2. Suggested C-S-H gel structure, illustrating bonds between and along sheets and polymerization of silicate chains.

particles of C_3S paste containing interlayers can be compacted together to form new bonds similar to those occurring within the interlayer system. In addition, there is evidence[11] that strong adhesion can form between C-S-H gel and $Ca(OH)_2$.

Using the compaction technique and by measurements of Young's modulus, Feldman[12] has studied the bonding between layers of cement gel when well pressed, partially separated or with water between them. Two series of compacted hydrated cement samples in the porosity range of 10–60% were made. Series B was made from bottle-hydrated Portland cement dried to 30% r.h., and series A, from the same material, made by d-drying (drying at 5×10^{-4} mm Hg). Figure 1.3 gives the sequence of exposure to water vapour of the two series of compacted samples, prepared at approximately 11% porosity. The values of Young's modulus at each condition are given.

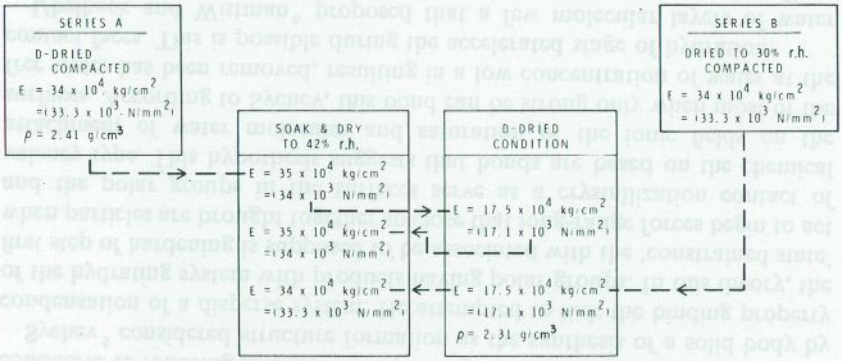

Figure 1.3. Sequence of conditioning and testing (ref. 12).

Both series B, compacted with interlayer water, and series A, compacted with interlayer water removed, give high and similar values of Young's modulus. However, in the d-dried series B, the modulus decreases by about 50%. No change occurs in the modulus values of series A samples on wetting but they, too, show a loss in modulus when dried. Compaction of the d-dried material brings layers close together, as shown in Fig. 1.4 in which density is plotted versus compaction pressure for both series: series A attains a density of 2.41 g/cm^3 as compared with 2.31 g/cm^3 for series B (d-dried). A higher Young's modulus in series A indicates that either some new bonds have been established or simply that the van der Waals' forces due to the proximity of the surfaces have also contributed to this increase. Calculations based on the densities show that the interlayer distance has become 0.5 Å less. Water seems to compensate for any decrease in Young's modulus when the layers move apart, which emphasizes the bridging role of water. It probably participates in

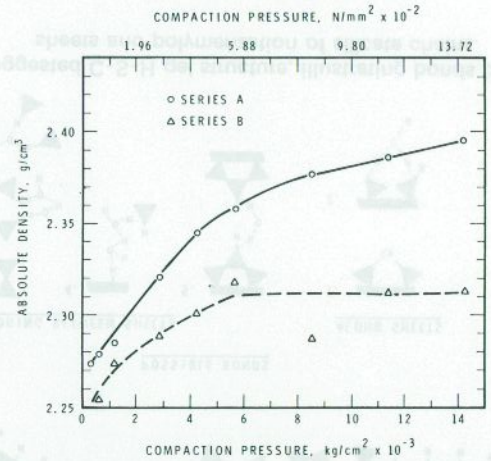

Figure 1.4. Density versus compaction pressure for bottle-hydrated cement (ref. 12).

bonding through several configurations, as shown in Fig. 1.2. Water also coordinates with calcium ions between the sheets.

The types of bonds discussed above imply that bonds between particles, originating from separate nuclei during hydration, can be similar to bonds within the particles. The concept of cement paste as a continuous mass around pores, when the paste is made at lower w/c ratios and is reasonably mature, rather than particles joined by special bonds, may be a more useful approach for formulating a model of cement paste. Thus, the area and type of contact may be the critical factor determining mechanical properties.

1.1.3. Absolute density

Traditionally, both density and porosity of hydrated Portland cement are measured in the d-dried state by pycnometric methods, using a saturated aqueous solution of calcium hydroxide as the fluid.[13] Since the d-dried hydrated Portland cement rehydrates on exposure to water, this method is of questionable value. More realistic values can be obtained by proper conditioning of the sample and using fluids that do not affect the structure of the paste. In Fig. 1.5, densities have been calculated using various simplified models of hydrated Portland cement paste. Table 1.1[13] shows the density values obtained using helium pycnometry, dried methanol and saturated aqueous $Ca(OH)_2$ solution. The density values were obtained for the bottle-hydrated cement at 11% r.h. and in the d-dry state. Values are given for each fluid and four

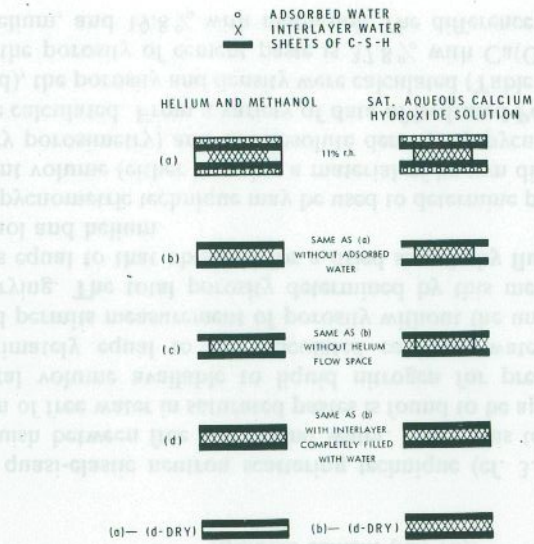

Figure 1.5. Schematic models for density calculations in Table 1.1 (ref. 13).

Table 1.1. Density of bottle-hydrated Portland cement

Condition 11% r.h.	Helium (g/cm^3)	Methanol (g/cm^3)	Saturated aqueous $Ca(OH)_2$ solution (g/cm^3)
(a) No correction	2.30 ± 0.015	2.25 ± 0.02	2.38 ± 0.01
(b) Monolayer adsorbed water correction	2.31 ± 0.015	2.26 ± 0.02	2.39 ± 0.01
(c) Helium flow taken into account	2.37 ± 0.015	2.32 ± 0.02	2.38 ± 0.01
(d) The interlayer space completely filled with water	2.34 ± 0.015	2.29 ± 0.02	2.35 ± 0.01
d-dry state			
(a) —d-dry	$2.28 + 0.01$	2.285 ± 0.02	2.61 ± 0.01
(b) —d-dry Calculation for layers themselves (uncorrected for free $Ca(OH)_2$)	2.51 ± 0.01 of paste (w/c ratio 0.8)		2.51 ± 0.01

different sets of values are shown for the 11 % r.h. condition. These values are different because of different conditions of exposure, and the models in Fig. 1.5 were used for calculations. In each model the density value is for the space surrounded by the heavy line. The same model is applicable for density determination by helium or methanol.

In Fig. 1.5, the density value for (a) includes adsorbed water and is calculated to be 2.30 g/cm^3. The value by helium is calculated, neglecting helium inflow between the layers. Methanol gives a value slightly lower than that by helium, partly because helium enters some portions of the layers into which methanol does not. The absolute density, using $Ca(OH)_2$ solution, was 2.38 g/cm^3. (The density of $Ca(OH)_2$ solution was taken as 1.0006 g/cm^3.)

In Fig. 1.5, using model (b), the density value is obtained by correcting for adsorbed water. The volume of adsorbed water was calculated using the N_2 surface area. Volume (c) is less than volume (b) because the helium inflow is taken into account. It is also assumed that water that had occupied the same space as in (a) had a density of 1.25 g/cm^3.[13] A correction is made for the density using $Ca(OH)_2$ solution and a value of 2.38 g/cm^3 for (c) is obtained compared with a value of 2.37 g/cm^3 by the helium method.

A calculation may also be made based on model (d). Using the solid volume of model (b) and adding the extra water, the density becomes 2.34 g/cm^3 by the helium method. The same model, (d), yields a value of 2.35 g/cm^3 by the $Ca(OH)_2$ solution method. By a proper accounting of the spaces, the same density values may be obtained by the helium and $Ca(OH)_2$ solution–pycnometric methods.

The results for the d-dried sample with helium and methanol are very close, while the value obtained with $Ca(OH)_2$ solution is higher. This is as expected since calcium hydroxide solution enters the interlayer and expands the material. The density of the layers themselves can also be calculated by excluding the volume and weight contributions of the interlayer water. This results in a value of 2.51 g/cm^3. This value, however, does not take into account any correction for free $Ca(OH)_2$.

1.2. NON-SOLID PHASE

1.2.1. Porosity

Porosity and pore distribution of solids are usually determined using mercury porosimetry and nitrogen or water vapour adsorption isotherms (cf. 1.2.2). The water adsorption isotherm technique has proved successful for materials with pore structures that remain stable on removal or addition of water.

Measurements for hydrated Portland cement, which is sensitive to stress, drying and exposure to different humidities, are difficult to interpret. Water

used as a medium on d-dried cement paste always gives higher porosity than that obtained using nitrogen, methanol or helium (Fig. 1.6).[13–15] The difference in porosity values can be explained by the decomposition of hydrates during drying. Hydrated Portland cement must be dried in order to measure its properties and this results in changes in porosity, surface area and other physical properties.[16–18] On exposure to water the dried material rehydrates.[19]

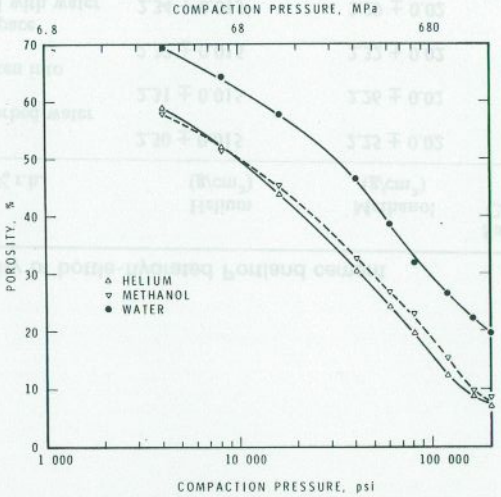

Figure 1.6. Relationship between porosity and compaction pressure for bottle-hydrated cement (ref. 13).

The quasi-elastic neutron scattering technique (cf. 3.4) has the ability to distinguish between free and bound water. Using this technique, the volume fraction of free water in saturated pastes is found to be approximately equal to the total volume available to liquid nitrogen for pre-dried pastes and is approximately equal to the calculated capillary water content.[19–21] This method permits measurement of porosity without the uncertainties associated with drying. The total porosity determined by this method for a saturated paste is equal to that obtained for a dried sample by fluids such as nitrogen, methanol and helium.

The pycnometric technique may be used to determine porosity. Knowing the apparent volume (either by using a material of known dimensions or by using mercury porosimetry) and the absolute density by pycnometry, pore volume may be calculated. From a variety of data of hydrated Portland cement pastes (d-dried), the porosity and density were calculated (Table 1.2).[22] At a w/c ratio of 0.4 the porosity of cement paste is 37.8% with $Ca(OH)_2$ solution, 23.3% with helium, and 19.8% with methanol. The difference on a volume/weight

basis is equivalent to 8.6 $cm^3/100$ g of d-dried cement. This compares well with the value estimated from scanning isotherms for interlayer water. The results lead to the general conclusion that porosity and absolute density of pastes are almost unchanged whether determined with helium or methanol; the values are higher with $Ca(OH)_2$ solution.

Table 1.2. Pore volume and density of d-dried hydrated cement pastes determined with different fluids

w/c ratio	Pore volume percentage (by volume)			Density (g/cm^3)			Surface area (N_2)
	Helium	Water	Methanol	Helium	Water	Methanol	
0.1	23.3	37.8	19.8	(i) 2.19 ± 0.015 (ii) 2.19 ± 0.015			$30\ m^2/g$
0.5	34.5	44.8	36.6		2.64 ± 0.06	2.27 ± 0.06	$55\ m^2/g$
0.6	42.1	51.0		(i) 2.28 ± 0.015 (ii) 2.26 ± 0.015	—	—	$51\ m^2/g$
0.8	53.4	59.5		(i) 2.30 ± 0.015 (ii) 2.27 ± 0.015	2.66 ± 0.06	—	$57\ m^2/g$
0.8 1.0	51.4	58.7	51.6	(i) 2.29 (ii) 2.26	2.61 ± 0.06	2.27	$57\ m^2/g$

1.2.2. Pore-size distribution

Mercury porosimetry

Mercury porosimetry involves forcing mercury into the vacated pores of a body by the application of pressure. If the pores are assumed to have a simple shape, an equation can be derived relating pore size to intrusion pressure. For cylindrical pores

$$d = \frac{-4\gamma \cos \theta}{P} \tag{1.1}$$

where P = applied pressure, d = pore diameter, γ = surface tension, and θ = contact angle of mercury on the pore wall.

The mercury porosimetry method enables the widest range of pore-size distributions to be measured. The upper diameter limit can be as high as 1000 μm; the lower limit can be as small as 30 Å, depending on the pressure and the contact angle used in the calculation.

A review of the porosimetry technique was published by Orr.[22] More recently, Liabastre and Orr[23] assessed the structure of a graded series of controlled pore glasses and Nucleopore membranes (both of which have pores

with right-cylinder characteristics) using both electron microscopy and mercury penetration. The data showed good agreement if a simple pressure correction was applied. It was suggested that pores are compressed to an hourglass shape, thereby exhibiting an effectively smaller diameter, until mercury actually enters them. Upon the entrance of mercury, the pores expand because of the equalization of hydrostatic pressure, and return to nearly their original volume. The partial closing and reduction in diameter accounts for the entry of mercury into pores apparently smaller than they actually are, and the subsequent return to shape explains correct volume measurements.

A survey of the method as applied to cement systems and some results for cement pastes at different w/c ratios was made by Winslow and Diamond.[24] It was observed that the pore volume left unintruded by mercury at 15 000 psi (102 MPa) was significantly less than the 28% that should represent gel pores.

Diamond and Dolch[25] investigated a separate class of 'gel pores' in the range of tens of ångströms, as postulated in the Powers' model. They showed that for a mature paste (318 days old) the pore volume, intruded below about 60 Å in diameter, is not only less than that predicted by a log normal plot, suggesting that all the pores intruded belong to a single pore-size distribution, but is almost negligible in absolute terms. The plot of cumulative percentage of pore volume intruded versus pore diameter for this sample is given in Fig. 1.7.[25] The total pore volume in this sample was measured as 0.306 cm^3/g. The volume intruded between pressure corresponding to pore diameters of 77 Å and 25 Å is only 0.011 cm^3/g.

In their study of capillary porosity, Auskern and Horn[26] showed that the addition of a small amount of water does not affect the porosity measured by mercury, contrary to the findings of Winslow and Diamond.[24] The porosity by mercury intrusion of an oven-dried sample up to 50 000 psi (340 MPa) was 0.108 cm^3/g; the oven-dried sample exposed to 5% r.h. had a porosity of

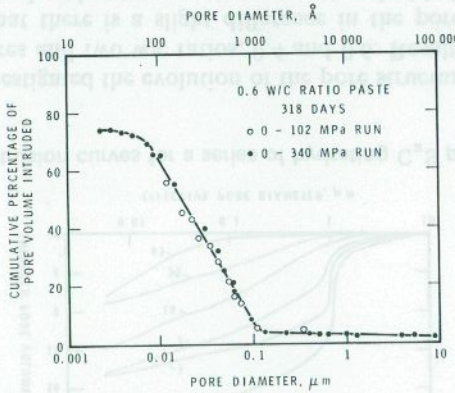

Figure 1.7. Cumulative mercury pore-size distribution for 0.6 w/c paste, 318 days old (ref. 25).

0.115 cm^3/g. This type of result was also observed by Beaudoin.[27] As a result, Auskern and Horn[26] used 117° as the contact angle for all their work. They also found limited penetration below about 80 Å and concluded that the 'missing porosity' relative to the porosity as determined by water adsorption must be explained by pores of diameter smaller than 35 Å. They found that the porosity measured by carbon tetrachloride saturation is close to, but slightly larger than, the porosity measured by mercury penetration. Beaudoin[27] measured total porosity by mercury porosimetry up to 60 000 psi (408 MPa) pressure and found that mercury porosimetry and helium pycnometric methods could be used interchangeably to measure porosity of cement paste if the w/c ratio was equal to or greater than 0.40. These results are shown in Fig. 1.8 (after ref. 27). Included in this figure is porous glass in which mercury was able to penetrate only 69% of the pore space. Average pore diameter of this material was measured by other techniques[28] to be between 50 and 60 Å.

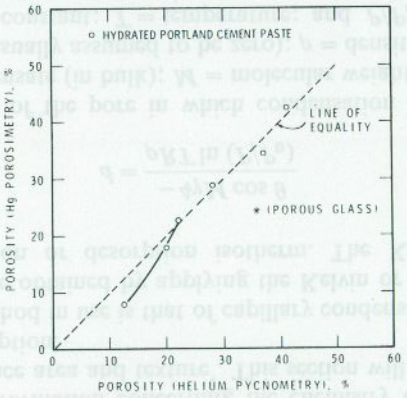

Figure 1.8. Mercury porosity versus helium porosity for hydrated Portland cement paste (ref. 27).

It is apparent that the results of the mercury porosimetry method agree with those of other techniques described previously, and especially with the helium inflow measurements. The results showed that the porosity was made up of a pore structure into which helium could rapidly enter, and of interlayer spaces of hydraulic radius less than 1 Å when the paste is oven dried.

In a study of capillary porosity during hydration of C_3S, Young[29] found that, on measuring the mercury intrusion, the pastes showed a threshold diameter that decreased with hydration; the results are shown in Fig. 1.9. This is in agreement with the finding of Winslow and Diamond.[24] It was suggested by Young that the large intrusion immediately below the threshold diameter (1000 Å) results from the filling of the void spaces between C-S-H gel needles, and the filling of larger pores accessible only through intergrowth of needles.

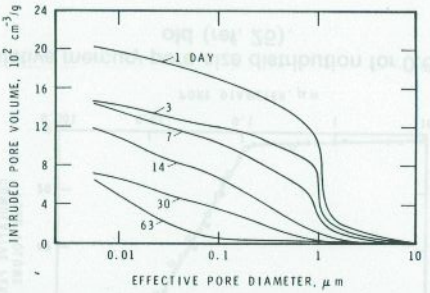

Figure 1.9. Intrusion curves for a series of hydrating C_3S pastes (ref. 29).

Diamond[30] investigated the evolution of the pore structure of cement paste at two temperatures and two w/c ratios, 0.4 and 0.6. Results for w/c = 0.6 in Fig. 1.10 show that there is a slight difference in the pore structure of the product formed slowly at low temperature as compared with that formed rapidly at higher temperature.[30] After about one year of hydration, the pore volume of the paste cured at 40 °C is higher than that cured at 6 °C because of the greater volume of pores smaller than 500 Å.

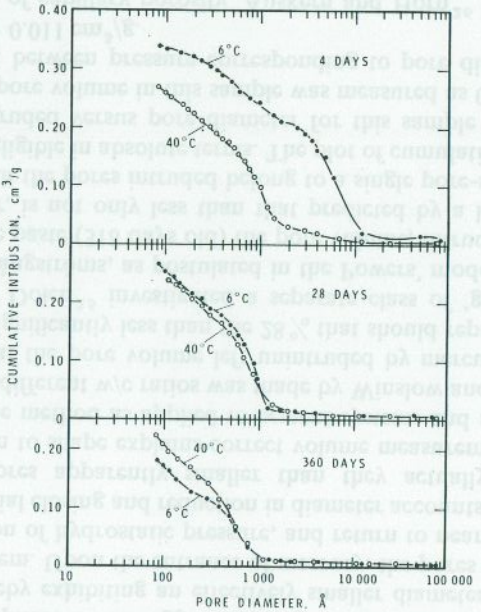

Figure 1.10. Cumulative pore-size distributions of 0.6 w/c cement pastes hydrated at 6 °C and at 40 °C (ref. 30).

Nitrogen adsorption and capillary condensation methods: comparison with mercury porosimetry

Adsorption of a vapour on a surface is considered to take place progressively, the thickness of the adsorbed film increasing with vapour pressure. At some stage, the thickness of the films on both sides of a pore approximate to the size of the pore, and 'capillary condensation' takes place; from these measurements pore structure analyses have been made.

Pore structure has been studied by the water-vapour adsorption method.[31–33] It has been shown in the previous sections that porosity determined by water is quite different from that determined by other fluids, largely because of the interaction of water molecules with the solid and their penetration into partially collapsed interlayer spaces. Several authors have now confirmed, however, 'that the high degree of specificity of water adsorption does not allow water vapour to be used as an alternative to nitrogen for determination of surface area and pore size distribution'.[34,35] It should, therefore, be exploited only to 'provide information concerning the chemistry of the solid surface rather than its surface area and texture'. This section will thus deal primarily with nitrogen adsorption.

The common method in use is that of capillary condensation. The pore-size distribution data are obtained by applying the Kelvin or similar equation to either the adsorption or desorption isotherm. The Kelvin equation for cylindrical pores is

$$d = \frac{-4\gamma M \cos\theta}{\rho RT \ln (P/P_0)} \tag{1.2}$$

where d = diameter of the pore in which condensation occurs; γ = surface tension of the condensate (in bulk); M = molecular weight of the condensate; θ = contact angle (usually assumed to be zero); ρ = density of the condensate (in bulk); R = gas constant; T = temperature; and P/P_0 = relative vapour pressure at which capillary condensation occurs.

A number of different assumptions as to pore shape and thickness of the adsorbed film at each stage have been used,[36–42] leading to some variation in calculation methods. However, in contrast to the wide range of sizes that can be determined by mercury porosimetry, capillary condensation methods are limited essentially to pores of diameters between a few tens to several hundreds of ångströms. The lower limit associated with capillary condensation methods depends on the particular isotherms, but it is generally accepted that the Kelvin equation tends to break down for micropores. Kadlec and Dubinin[43] presented data suggesting that the Kelvin equation does not apply for pore diameters as small as 35–40 Å. They concluded that this equation is inapplicable at relative vapour pressures slightly higher than those at which the adsorption–desorption hysteresis loop closes, and appears to be a characteristic of the adsorbate. The limiting diameters range from 20 to 35 Å for various adsorbates.

Recently, Winslow[44] reported results that showed satisfactory agreement between mercury porosimetry and nitrogen adsorption for porous alumina in the pore range 40–500 Å.

In a comprehensive study of a variety of pastes of Portland cement and C_3S, Bodor *et al.*[45] found a maximum for the pore-size distribution at around 12 Å hydraulic radius, i.e. 48 Å diameter with the assumption of cylindrical pores. Bodor also stated that no micropores are measured in hydrated Portland cement by this technique nor by the 't-method'. In a review, Diamond[46] observed that most plots in the literature display strong maxima between 30 and 50 Å. However, he observed that the cumulative volume determined by mercury intrusion was not too different from that by capillary condensation for pores of 100–400 Å in diameter; below 100 Å this was not the case. The capillary condensation data obtained by some workers show steep slopes and considerable pore volume below 100 Å and particularly below 50 Å. This fact led Diamond[46] to suggest that large amounts of the C-S-H were encapsulated by calcium hydroxide and unintrudable by at least mercury, but the work of Auskern and Horn[26] and the helium pycnometric work dispels this idea and, in any event, the pore-size distribution by mercury intrusion should still be reasonably representative of the whole of the distribution. Diamond[46] used radius of gyration results obtained by Winslow[44] in his low-angle X-ray scattering work, and calculated mean diameters, assuming various models. He obtained a mean diameter of approximately 300 Å assuming a cylinder of equal length and diameter. Mikhail *et al.*[47] later refuted this work on the basis that the calculated surface area was too low. They used both radius of gyration and hydraulic radius to calculate the dimensions of an average cylindrical pore and obtained a diameter of 47.2 Å and a length of 466 Å. These authors, however, had obtained their hydraulic radius by water adsorption which, as stated previously, leads to errors.

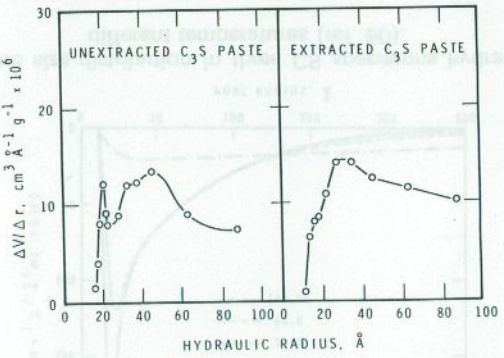

Figure 1.11. Pore-size distribution derived from adsorption isotherms (adsorption branches of N_2 isotherms were used for calculation) (ref. 48).

Recent work by Daimon *et al.*[48] presented results on leached and unleached C_3S. Accordingly, the pore volume of an unextracted $Ca(OH)_2$ sample should be multiplied by 1.43 to compare it with the extracted paste. It was found that the pore volume determined by nitrogen adsorption was 1.39 times the values of the unextracted pastes, suggesting that $Ca(OH)_2$ does not engulf any appreciable volume of C-S-H. Work by Feldman and Ramachandran[49] with the helium flow technique leads to the same conclusion.

The pore-size distributions obtained by Daimon *et al.*[48] are presented in Fig. 1.11 and Table 1.3. In this table, there are columns for the calculation of pore distribution using both the adsorption and desorption isotherm, and for parallel plate (surface area and pore volume, S_{pp}, V_{pp}) or cylindrical pores (S_{cp}, V_{cp}). Best fit is given by the adsorption curve, and both models give a reasonable fit, although the cylindrical model is better for the extracted paste. This is determined[49] by comparing calculated values with S_{BET}, surface area determined by the BET (Brunauer–Emmett–Teller) method, and V_p, the total porosity, in the upper part of Table 1.3. The hydraulic radius gives the pore diameter down to about 60 Å, assuming a cylindrical model.

Table 1.3. N_2 adsorption data

Parameter	Unextracted C_3S paste		Extracted C_3S paste	
V_m (cm^3/g)	4.177		8.135	
S_{BET} (m^2/g)	18.17		26.69	
S_t (m^2/g)	17.5		25.5	
V_p (ml/g)	0.1342		0.1862	
	Adsorption	Desorption	Adsorption	Desorption
S_{pp} (m^2/g)	18.09	33.43	24.32	43.78
S_{vp} (m^2/g)	21.09	42.00	28.53	48.37
V_{pp} (ml/g)	0.1340	0.1412	0.1832	0.1942
V_{cp} (ml/g)	0.1358	0.1453	0.1851	0.1994

Results by Collepardi[50] show that pore-size distribution by nitrogen capillary condensation of room temperature-cured C_3S paste has a maximum at about 20 Å pore radius, although the average appears to be at a much higher value. These results are plotted in Fig. 1.12 as the differential, $\Delta V/\Delta r$, of the plot of pore radius (r) against the total volume (V) of pores with greater radius than r. It is also shown, by hydrating at different temperatures, that the reduction in pore volume is due almost exclusively to the decrease in volume of the smaller pores, down to about 60 Å radius. These results show general agreement with mercury intrusion, although nitrogen capillary condensation techniques indicate, in some cases, greater volumes in small pores. This difference may be explained, however, by the fact that t-curves, the variation of film thickness with relative pressure, are important in the calculation of the small pore distribution, and measuring the appropriate t-curve is difficult for hydrated Portland cement. In addition, the validity of their application for small pores is debatable.

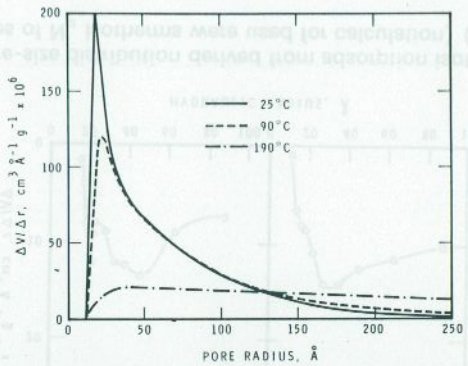

Figure 1.12. Pore size distribution in three CS specimens hydrated for 1 day at different temperatures (ref. 50).

1.3. HYDRAULIC RADIUS AND SURFACE AREA

Porosity of the d-dried cement paste measured by helium pycnometry is similar to that referred to as capillary porosity,[21] while the value obtained by $Ca(OH)_2$ solution includes the space partially created by the penetration of a water solution into interlayer spaces. The average characteristics of both these 'porosities' can be represented by the term 'hydraulic radius', which is obtained by dividing the total pore volume by the total bounding surface area.

1.3.1. Pore system

When d-dried hydrated Portland cement is exposed to low water vapour pressure, the water molecules enter the pores, adsorb on the walls of the pores, and some molecules also penetrate the layered structure within the solid. The solid particles swell, not only because of the interlayer penetration, but also by the physical interaction of water on the surface of the solid. The latter interaction causes Bangham swelling (cf. 3.4) and is due to a decrease in the surface energy forces that compress the solid in the dry state. The overall swelling should be transmitted through the porous body and is measured as $\Delta l/l$ (Δl = length change, l = initial length) which represents the linear expansion of the porous body. If $\Delta l/l$ is small, $3\Delta l/l$ would be equivalent to the volumetric expansion. If there is no change in porosity or packing of particles during different exposure conditions, then $3\Delta l/l$ is equal to the fractional volume change of the solid phase of the body.

A measurement of the solid volume (of cement paste exposed to a particular humidity) by helium pycnometry would include the adsorbed water, as well as the solid in the expanded state. By measuring the solid volume at the d-dried state and at 11 % r.h., where the adsorbed water is approximately equal to a monolayer, the volume of a monolayer of adsorbed water plus the increase of the volume of the solid can be determined. This is referred to as $\Delta V/V$ (where ΔV = the change in solid volume from the d-dried state to 11 % r.h. and V = solid volume at the d-dried state). The difference of the volume changes would then be equal to the volume of the adsorbed water as a fraction of the total volume of the solid. This may be expressed as

$$\Delta V/V - 3\Delta l/l = v/V \tag{1.3}$$

where v is the volume of the adsorbed water and V the volume of the solid.[51] The measurement of both these volume changes assumes that during the change of condition from 0 to 11 % r.h. little or no ageing occurs. Previous work has shown this assumption to be valid.[52]

Because v is the volume of the monolayer of adsorbed water on the internal surface of the pore space, surface area can be calculated. The hydraulic radius of a pore system is computed by dividing the total pore volume of the system by its surface area and is shown in Table 1.4 for hydrated Portland cement paste prepared at w/c = 0.4, 0.6 and 0.8.

Table 1.4. Surface area and hydraulic radius of hydrated Portland cement by helium pycnometry

w/c ratio	Surface area (m^2/g)	Hydraulic radius (Å)
0.4	35.0	39.4
0.6	49.0	64.2
0.8	44.0	107.0

Using this method, surface areas were determined for ten different samples of hydrated Portland cement and C_3S of various w/c ratios. These values were plotted against surface area values determined by nitrogen adsorption, using the same drying technique (Fig. 1.13).[53] Although some deviation occurs at lower surface areas, the agreement justifies the general validity of the equation. The results demonstrate the validity of the concept that the instantaneous helium pore volume is the same as that determined by nitrogen, and that the remaining pore volume is that of the partially collapsed interlayer space. These results confirm the conclusions drawn from applying the inelastic neutron scattering technique.

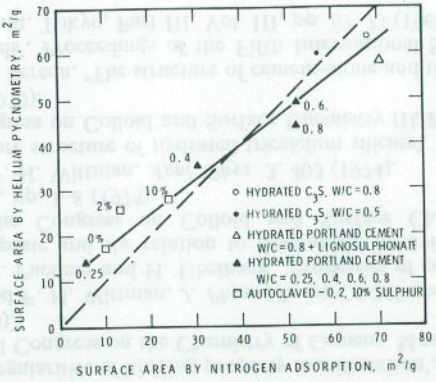

Figure 1.13. Surface area by nitrogen adsorption and by helium pycnometry (ref. 53).

1.3.2. Interlayer space

Hydraulic radius calculation for the interlayer space requires the surface area of the interlayer space and the corresponding volume. The low-angle scattering data of Winslow and Diamond[54] have provided some indication of the surface area value in the wet state. In a d-dried paste, the interlayer space is reopened by exposure to 42% r.h.; at this condition helium can fully enter the interlayer space within 40 h of flow time so that the volume of the interlayer space can be measured in the partially-open or fully-open state, depending on the relative humidity of exposure.

In a hydrated cement paste cured at a w/c ratio of 0.6, and exposed to 100% r.h., the helium volume-change method gives a value of 1.35% water for the monolayer on the external surface (corresponding to a surface area of 49 m^2/g). This sample at 11% r.h. retains 10.8% water.[55]

This leaves $10.8 - 1.35 = 9.45\%$ in the interlayer structure. A space of 2.4 cm^3 unoccupied by water was also measured in the interlayer structure by helium inflow. Using 1.20 g/cm^3 as the density of the water results in a volume of 10.28 cm^3 as the internal space. The surface area for the total space is 670 m^2/g, determined by Winslow and Diamond,[54] resulting in $670 - 49 = 621$ m^2/g for the interlayer surface, and a hydraulic radius of 1.65 Å.

Assuming that the pores are bounded by two parallel plates, the average separation between the plates is 3.3 Å (twice the hydraulic radius). This model is consistent with the internal system composed of layers separated by, on average, one water molecule. The impact of this calculation may be shown by another simple calculation. If 9.45% of water is held as a single layer between two sheets, it will cover twice the normal area per molecule, i.e. 10.8×2 $Å^2$ (0.216 nm^2). This results in a surface area of 687.2 m^2/g compared with 621 m^2/g

given by low-angle X-ray scattering. This, however, assumes that all the water is held as a single layer, while in fact there may be 'kinks' in the alignment of the sheets, leaving room for more than one layer of water.

The hydraulic radius can also be calculated for the sample when exposed only to 42% r.h. and where 5.15% water and 2 cm^3 of space exist between the sheets: this gives an average hydraulic radius of 1.0 Å, obviously a result of a partially collapsed state.

Calculations of this type have also been obtained from the data of Brunauer *et al.*[56] and Mikhail and Abo-El-Enein.[57] In these cases, the internal volume was obtained by measuring the difference between the total water and the total nitrogen porosity; the surface areas were determined by the difference between the surface areas given by Winslow and Diamond[54] and the surface area determined by nitrogen adsorption.

The results calculated from the data of Brunauer *et al.*[56] are shown in Table 1.5; an average hydraulic radius of 1.23 Å was obtained for the four pastes at

Table 1.5. Surface areas, porosities and hydraulic radii of Portland cement paste

w/c ratio	S_{N_2} (m^2/g)	$S_T - S_{N_2}$ (m^2/g)	$V_{H_2O} - V_{N_2}$ (ml/g)	$\frac{V_{H_2O} - V_{N_2}}{S_T - S_{N_2}}$ (Å)	
0.35	56.7	580 – 56.7	0.0516	0.99	
0.40	79.4	642 – 79.4	0.0717	1.28	av. = 1.23
0.50	97.3	642 – 97.3	0.0823	1.51	
0.57	132.2	670 – 132.2	0.0617	1.14	

w/c ratios between 0.35 and 0.57. In the table, S and V refer to the surface area and pore volume, with the fluid used as the subscript. S_T is the total surface area determined by low-angle scattering.

In Table 1.6, the data of Mikhail and Abo-El-Enein,[57] corrected for degree of hydration, give an average value of 2.51 Å when the first value at 18.50% hydration is excluded. These data were obtained for pastes cured at a w/c ratio

Table 1.6. Internal radius of low porosity pastes

Sample No.	Degree of hydration (%)	$V_{H_2O} - V_{N_2}$	$676 - S_{N_2}$ (m^2/g)	Hydraulic radius (Å)	
I	18.50	0.92	644	14.4	
II	33.80	0.175	628	2.78	
III	49.30	0.144	646	2.22	
IV	57.1	0.155	655	2.36	av. = 2.51
V	62.0	0.184	667	2.78	
VI	74.1	0.168	668	2.51	
VII	78.1	0.166	671	2.48	

of 0.2. This value is much higher than that obtained from the other data (Table 1.5) but is consistent with other results for low w/c ratio pastes. Very low surface areas[57] and relatively low densities[58] are obtained for these pastes, and it must be concluded that there are many 'kinked' regions in the stacking of the sheets and trapped space, due to lack of space during hydration. This is illustrated in Fig. 1.14, a further modification by Daimon *et al.*[48] based on the model by Feldman and Sereda.

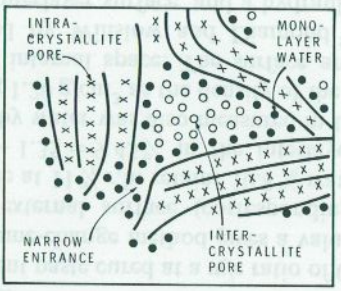

Figure 1.14. Modification of Feldman and Sereda model (ref. 48).

REFERENCES

1. O. E. Radczewski, H. O. Muller and W. Eitel, *Naturwissenschaften* **27**, 807 (1939).
2. V. S. Ramachandran and R. F. Feldman, *J. Appl. Chem. Biotechnol.* **23**, 625 (1973).
3. P. J. Sereda and V. S. Ramachandran, *J. Am. Ceram. Soc.* **58**, 249 (1975).
4. P. A. Rehbinder, E. E. Segalova, E. A. Amelina, E. P. Andreeva, S. I. Kontorowich, O. I. Lukyanova, E. S. Solovyeva and E. D. Shchukin, 'Physico chemical aspects of hydration hardening of binders', Proceedings of the Sixth International Congress on the Chemistry of Cement, Moscow, Vol. II, Book 1, pp. 58–64 (1974).
5. M. M. Sychev, 'Regularities of binding property manifestation', Proceedings of the Sixth International Congress on the Chemistry of Cement, Moscow, Vol. II, Book 1, pp. 42–57 (1974).
6. H. J. Ubelhack and F. H. Wittman, *J. Phys.* (*Paris*) C6-269 and C6-273 (1976).
7. F. H. Wittman, U. Puchner and H. Ubelhack, 'Properties of colloidal particles in hardened cement paste and the relation to mechanical behaviour', International Proceedings of the Congress on Colloid and Surface Chemistry (IUPAC), Budapest/Ungarn., pp. 1–8 (1975).
8. M. J. Setzer and F. H. Wittman, *Appl. Phys.* **3**, 403 (1974).
9. M. Collepardi, 'Pore structure of hydrated tricalcium silicate', Proceedings of the International Congress on Colloid and Surface Chemistry (IUPAC), Prague, Vol. 1, pp. B25–B49 (1973).
10. I. Soroka and P. J. Sereda, 'The structure of cement-stone and the use of compacts as structural models', Proceedings of the Fifth International Symposium on the Chemistry of Cement, Tokyo, Part III, Vol. III, pp. 67–73 (1968).

11. B. Marchese, *Cem. Concr. Res.* **7**, 9 (1977).
12. R. F. Feldman, *Cem. Concr. Res.* **2**, 375 (1972).
13. R. F. Feldman, *Cem. Technol.* **3**, 3 (1972).
14. R. Sh. Mikhail, L. E. Copeland and S. Brunauer, *Can. J. Chem.* **42**, 426 (1964).
15. R. F. Feldman, 'Volume change, porosity and helium flow studies of hydrated portland cement', Proceedings of the RILEM/IUPAC International Symposium on Pore Structure and Properties of Materials, Prague, Vol. 1, pp. C101–116 (1973).
16. G. G. Litvan, *Cem. Concr. Res.* **6**, 139 (1976).
17. R. F. Feldman and V. S. Ramachandran, *Cem. Concr. Res.* **4**, 155 (1974).
18. R. F. Feldman, *Cem. Concr. Res.* **4**, 1 (1973).
19. D. H. C. Harris, C. G. Windsor and C. D. Lawrence, *Mag. Concr. Res.* **26**(87), 65 (1974).
20. R. A. Helmuth and D. H. Turk, *Highw. Res. Board Spec. Rep.* **90**, 135 (1966).
21. G. J. Verbeck and R. A. Helmuth, 'Structures and physical properties of cement pastes', Proceedings of the Fifth International Congress on the Chemistry of Cement, Tokyo, Vol. III, pp. 1–32 (1968).
22. C. Orr, *J. Powder Technol.* **3**, 117 (1970).
23. A. A. Liabastre and C. Orr, *J. Colloid Interface Sci.* **64**, 1 (1978).
24. D. N. Winslow and S. Diamond, *ASTM J. Mater.* **5**, 564 (1970).
25. S. Diamond and W. Dolch, *J. Colloid Interface Sci.* **38**, 234 (1972).
26. A. Auskern and W. Horn, *ASTM J. Test. Eval.* **1**, 74 (1973).
27. J. J. Beaudoin, *Cem. Concr. Res.* **9**, 771 (1979).
28. C. H. Amberg and R. McIntosh, *Can. J. Chem.* **30**, 1012 (1952).
29. J. F. Young, *J. Powder Technol.* **9**, 173 (1974).
30. S. Diamond, 'Pore structure of hardened cement paste as influenced by hydration temperature', Proceedings of the RILEM/IUPAC International Symposium on Pore Structure and Properties of Materials, Prague, Vol. 1, pp. B73–88 (1973).
31. R. Sh. Mikhail, S. Brunauer and E. E. Bodor, *J. Colloid Interface Sci.* **26**, 45 (1968).
32. J. Hagymassy and S. Brunauer, *J. Colloid Interface Sci.* **33**, 317 (1970).
33. J. Hagymassy, I. Odler, M. Yudenfreund, J. Skalny and S. Brunauer, *J. Colloid Interface Sci.* **38**, 20 (1972).
34. R. Sh. Mikhail, S. Nashed and K. S. W. Sing, 'The adsorption of water by porous hydroxylated silicas', Proceedings of the RILEM/IUPAC International Symposium on Pore Structure and Properties of Materials, Prague, Vol. 4, pp. C157–164 (1973).
35. K. S. W. Sing, 'A discussion of the paper "Complete pore structure analysis" by S. Brunauer, J. Skalny and I. Odler', Proceedings of the RILEM/IUPAC International Symposium on Pore Structure and Properties of Materials, Prague, Vol. 4, pp. C209–210 (1973).
36. E. P. Barrett, L. G. Joyner and P. P. Halenda, *J. Am. Chem. Soc.* **73**, 373 (1951).
37. C. Pierce, *J. Phys. Chem.* **57**, 149 (1953).
38. W. P. Innes, *Anal. Chem.* **29**, 1069 (1957).
39. R. W. Cranston and F. A. Inkley, *Adv. Catal.* **9**, 143 (1957).
40. D. Dollimore and G. R. Heal, *J. Appl. Chem.* **14**, 109 (1964).
41. B. F. Roberts, *J. Colloid Interface Sci.* **23**, 266 (1967).
42. S. Brunauer, R. Sh. Mikhail and E. E. Bodor, *J. Colloid Interface Sci.* **24**, 451 (1967).
43. O. Kadlec and M. M. Dubinin, *J. Colloid Interface Sci.* **31**, 479 (1969).
44. D. Winslow, *J. Colloid Interface Sci.* **67**, 42 (1978).
45. E. E. Bodor, J. Skalny, S. Brunauer, J. Hagymassy and M. Yudenfreund, *J. Colloid Interface Sci.* **34**, 560 (1970).
46. S. Diamond, *Cem. Concr. Res.* **1**, 531 (1971).
47. R. Sh. Mikhail, D. Turk and S. Brunauer, *Cem. Concr. Res.* **5**, 433 (1975).